Theoretical Study on X−H, −O, −OH, −NO, −ONO, and $-NO_2$ (X = CH_3, *t*-C_4H_9, $C_{13}H_{21}$)

H. T. Thümmel[†]

NASA Ames Research Center, Moffett Field, California 94035-1000

Received: June 9, 1997; In Final Form: October 8, 1997

Theoretical studies are reported for conformational energies and bond energies of compounds X−H, X−O, X−OH, X−NO, $X-NO_2$ X−ONO, XO−NO, and XN(O)−O with X = CH_3, *tert*-butyl, and $C_{13}H_{21}$, which are templates for a radical site of a hydrogen-terminated diamond C(111) surface. All structures are fully optimized using density functional theory (DFT) based on the B3LYP functional. For X = CH_3 calibration calculations are done in detail using the coupled-cluster approach (CCSD(T)) and do support use of the B3LYP functional for rotational barriers and bond energies. Bond energies X−O and X−OH for X = *tert*-butyl are close to those computed for X = $C_{13}H_{21}$, but bond energies X−NO, $X-NO_2$, X−ONO, and XO−NO differ by 5−11 kcal/mol and show that the effect of second nearest neighbors of the surface is significant in these cases. Combining the trends observed for the small cluster models yields our best values for adsorption energies on an active site of hydrogenated C(111): Bond energies decrease in the sequence C−H (98 kcal/mol) > C−OH (95 kcal/mol) > C−O (94 kcal/mol) > trans C−ONO (53 kcal/mol) > $C-NO_2$ (53 kcal/mol) > cis C−ONO (45 kcal/mol) > C−NO (30 kcal/mol). Dissociation energies of cis CO−NO and trans CO−NO are small (26 kcal/mol, 33 kcal/mol). All barriers computed for internal rotation along C−N and C−O are less than 1 kcal/mol, which shows that the rotation of adsorbed species is essentially free.

1. Introduction

With the need for faster computers several ideas have been proposed. One idea is to build electronic devices based on thin sheets of diamond, which may be many times faster than their silicon counterparts. Further, the unique properties of diamanoid materials such as wide band gap, high thermal conductivity radiation and chemical inertness, high C−C bond energies, and negative electron affinity[1] envisage diamond materials for challenging applications in high-temperature electronics, for harsh conditions or long time stability of electronic devices. For example, robust, cold diamanoid cathodes[2] could increase the lifetime of satellites since the (conventional) high-power traveling wave tubes tend to wear out with time.[3]

In silicon etching, reactive fluorine plasmas are primarily used to etch away a silicon surface. For carbon materials other techniques are required. Oxygen atoms or oxygen-containing molecules are commonly used etchants for graphite,[4] polymers,[5] and diamond films,[4,6−9,11] removing layers of carbon atoms from the surface while forming volatile compounds such as CO(g) and CO_2(g). Further, the presence of oxygen in the plasma is of interest in the CVD synthesis of diamond since it has been shown that a portion of oxygen added to the supply gases strongly affects the growth process and quality and can reduce surface defects.[12−14] Accurate chemisorption energies and adsorbate−surface potential parameters are required for simulating plasma surface interactions and obtaining structural relationships for etching and processing diamanoid semiconductors.

It is known that the adsorption energy of O_2 on diamond is small and requires much energy to start the etching process, which requires harsh conditions that may damage the device. Therefore it has been argued to use NO_2 instead of O_2, which is known to have a higher adsorption energy and has been reported to yield a 10 times larger etching rate under mild conditions (T = 298 K).[6] It is clear that in principle all species of an oxygen plasma reacting with a diamond surface (products CO, CO_2, H_2O, ···, free radicals H, O, OH, ···, metastable species, ions), reactive or nonreactive, can participate in the etching process, under the conditions of being chemisorbed on the surface with a reasonable rate.[16,17] Neglecting the ions, we expect strong surface bonding for atomic H, O, and oxygen-containing radicals such as OH and NO_2.

We should note that there is also a need for data of the interaction of radicals such as NO_2 and also NO with silicon or similarly diamond surfaces to build NANO devices for storage of data.[18] Recently Bauschlicher et al.[19] have suggested using strong covalent bonds for atomwise storage of data and have focused on surface−H and surface−F bonds. Starting with a hydrogen-passivated surface, the data could be written by selectively replacing H by F atoms, whereby in the first step individual H atoms could be removed via an STM tip.[20] However, the big problem in the subsequent F deposition is the formation of destructive radicals, which may destroy the data integrity, as is expected if strong fluorination agents such as F_2 or XeF_2 are used. Therefore, we have looked for milder fluorination agents.[21] For FNO_2[21] and FNO[22] we have shown that these species will be dissociatively adsorbed on C(111) with a sufficiently small barrier of less than about 10 kcal/mol. Nevertheless, the presence of NO or NO_2 interacting with the surface will create appropriate conditions and speed data collection primarily to circumvent unwanted surface reactions. Thus, in addition to etching there is potential tribology interest for accurate data on $C-NO_2$, C−ONO, and C−NO.

Since experimental data are unavailable, ab initio calculations must be used. We report conformational energies and bond energies C−Y with Y = H, O, OH, NO, ONO, and NO_2 for the hydrogenated diamond C(111) surface.

[†] Permanent and present address: PTECH Engineering GmbH, Östingstr. 13, 59063 Hamm, Germany.

S1089-5639(97)01873-2 CCC: $15.00
Published on Web 02/24/1998

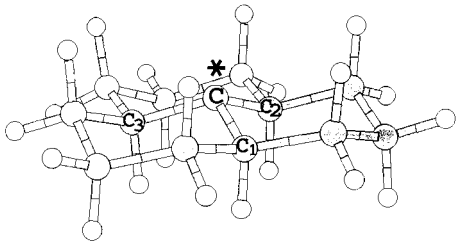

Figure 1. The $C_{13}H_{21}$ cluster, which is our most accurate model for the hydrogenated diamond (111) surface. The radical site is denoted by a star.

2. Model

In practice, the amount of etching will depend on the number of dangling bonds, the angle of the terminating H bonds, and the roughness of the surface, i.e., the preparation[23] and cleaning of the surface and properties of the interacting plasma. It is known that for a hydrogenated diamond C(111) surface the position of carbon atoms at the surface is close to the position for bulk terminated C(111).[24] Further, though the C−H bond energies are not known, it has been shown that high temperatures (1000−1300 K) are required to desorb the hydrogens.[24,25] For bonding sites of a diamond surface, one ideally would use a code that includes translational symmetry, but this is less ideal for localizing stationary points of the potential hypersurface, and determining C−Y bond energies and frequencies since it is in general based on SCF or DFT methods and we want to be able to use higher levels of theory that are computationally affordable if we use cluster models. It is known that for metals there are large edge effects, and large clusters are required for studying chemisorption. On the contrary, if we are interested in surface bonding of diamond, we expect, similar to covalent bonding of substituted hydrocarbons,[26] rapid convergence with increasing size of the cluster model, thus making the cluster approach very well-suited.

The simplest model for a radical site of C(111) with a σ dangling orbital is CH_3, and it is sufficiently small to allow accurate calibration calculations. The biggest effect missing is the effect of neighboring C_nH_m groups. The possible magnitude of this effect on C−Y bond energies can be estimated from accurate data for hydrocarbons, when available. For example, C−H bond energies decrease by 3−8 kcal/mol[27,28] when substituting the H atoms of the CH_3 model by small alkyl groups and show that the radical is stabilized relative to the corresponding C−Y compound for Y = H due to charge donation.

The next cluster is *tert*-butyl, where the bonding site has three neighboring CH_3 groups. On the basis of alkane C−H bond energies we expect similarly to atomic hydrogen that for atomic oxygen the C−O bond energy for *tert*-butyl is close to the adsorption energy on a C(111) radical site. However, for molecules Y = OH, NO, and NO_2 the *tert*-butyl model neglects any steric effects between the surface and Y. This limitation is removed for our largest cluster model $C_{13}H_{21}$ (Figure 1), where neighboring surface atoms of hydrogenated diamond C(111) are also included.

3. Methodology

The geometries are fully optimized and the frequencies computed at the optimal geometry using DFT based on the B3LYP[29] functional. The B3LYP calculations are calibrated using the coupled-cluster singles and doubles approach[30] including a correction for unlinked triple excitations,[30] CCSD(T). Most calculations are performed using the basis sets developed by Pople and co-workers.[32] Some calculations are performed using the correlation-consistent polarized valence (cc-pV*n*Z) sets developed by Dunning and co-workers[33] of double, triple, and quadruple zeta quality denoted as cc-pVDZ, cc-pVTZ, and cc-pVQZ. While the CCSD(T) method is known to yield a very accurate description of the correlation problem, it is also known to require very large basis sets to reach the one-particle basis set limit. To overcome this limitation, we use a modified G2[34] approximation, namely, the G2(B3LYP/MP2/CC) approach.[34] For simplicity, we denote this as G2′(MP2). In this approach the geometry and zero-point energy (ZPE) are determined at the B3LYP level of theory using the 6-31G* basis set; to calculate the zero-point energy, the B3LYP harmonic frequences are scaled by 0.98.[34] At this geometry, the energies are calculated at the MP2/6-311G**, MP2/6-311+G(3df,2p), and CCSD(T)/6-311G** levels of theory. The final energy, E(G2′(MP2)), is obtained as E(CCSD(T)/6-311G**) + E(MP2/6-311+G(3df,2p)) − E(MP2/6-311G**) + ZPE + HLC, where HLC is the higher level correction, which is based on the number of valence α and β electrons and determined by minimizing the computed error in the atomization energies of 55 molecules where the experimental values are well-known. For simplicity, we will denote the MP2 estimate for the basis set incompleteness, E(MP2,extended basis) − E(MP2,6-311G**), as ΔMP2.

The present study is based on the GAUSSIAN 94 package of computer programs;[36] in some cases when employing the Dunning basis sets the calculations have been performed using the MOLPRO code.[37,38]

4. Results and Discussion

4.1. CH_3 + O, OH, NO, and NO_2. The geometries are optimized and harmonic frequencies are computed at the B3LYP level of theory. B3LYP geometries were found in good agreement with experimental data, when available, as has been found in many other cases.[39] Energies are calibrated using more accurate levels of theory (Tables 1 and 2). The available experimental data[26,41,48−55] is also included in the tables. B3LYP has better agreement with G2′(MP2) values than CCSD(T) results for these compounds (Table 1). This is encouraging, since the B3LYP calculations are significantly less costly. The differences between the CCSD(T) and CCSD(T) + ΔMP2 results are between 5 and 10 kcal/mol and indicate that the MP2 estimate for basis set incompleteness is important for the bond energies considered. Major computational effort is necessary to achieve an accuracy beyond the G2′(MP2) level of theory. For the bond energy CH_3−O we also have performed some CCSD(T) calculations increasing the size of the one-particle basis employing Dunning's correlation consistent sets cc-pV*n*Z up to quadruple-ζ quality, cc-pVQZ (Table 2). Using basis set extrapolation to cc-pV∞Z, as described in ref 40, yields our best D_e value of 92.0 kcal/mol, in good agreement with the G2′(MP2) result (93.3 kcal/mol). We estimate a remaining uncertainty less than 2 kcal/mol, where the primary source could be typically[40] due to the neglect of core correlation rather than spin−orbit effects or taking B3LYP geometries or the error in reaching basis set completeness within the CCSD(T) approach for treating the electron correlation. The cc-pV∞Z value is 1.5 kcal/mol larger than the CCSD(T) + ΔMP2 result and suggests that the MP2 basis set incompleteness correction to the G2′(MP2) approach is somewhat too small. However, the G2′ result is larger by 1.3 kcal/mol. Thus the semiempirical higher level correction (HLC) to the G2′ approach lowers this deficiency in some way.

The direct computation of bond energies to chemical accuracy is costly even for a small molecule like CH_3O. However, as

TABLE 1: Calibration Calculations for Bond Energies CH_3-O, $-OH$, $-ONO$, and $-NO_2$. The B3LYP Values Are Computed with the 6-31G* Basis Set, Whereas the 6-311G Set and cc-pVTZ Are Used in the CCSD(T) Calculations. ΔMP2 Is the MP2 Basis Set Incompleteness Contribution to the G2′ (MP2) Approach**

D_e (kcal/mol)

structure	B3LYP	CCSD(T) 6-311G**	CCSD(T) +ΔMP2	G2′ (MP2)	CCSD(T) VTZ
H_3C-NO_2	62.02	60.87	66.45	69.16	
H_3C-NO	42.62	38.75	42.25	44.96	41.14
H_3C-O	95.10	82.95	90.55	93.26	87.71
H_3C-ONO cis	61.16	60.69	64.12	66.83	62.82
H_3C-ONO trans	59.58	59.27	63.08	65.79	
H_3C-OH	95.80	92.37	97.80	100.51	95.44
$H_3CN(O)-O$	96.85	84.21	95.46	98.17	
H_3CO-NO cis	43.51	39.82	44.83	47.54	43.81
H_3CO-NO trans	41.94	38.55	43.79	46.50	
ΔE(cis−trans)	1.58	1.42	1.04	1.04	
$\Delta E(XNO_2-XONO)$	0.86	0.19	2.33	2.33	

D_0 and D_{298} (kcal/mol)

	B3LYP		G2′(MP2)		
structure	0 K	298 K[a]	0 K	298 K[a]	expt
H_3C-NO_2	54.93	56.57	62.07	63.71	60.1(298 K)[b]
H_3C-ONO cis	54.89	56.53	60.55	62.19	58.2(298 K)[b,c]
H_3C-ONO trans	53.53	54.98	59.74	61.19	(57.2(298 K))
H_3C-NO	37.01	38.67	39.35	41.01	40.0 ± 0.8(298 K)[d]
H_3C-O	90.82	91.92	88.99	90.09	88.7(0 K), 90.8(298 K)[e]
H_3C-OH	87.59	89.55	92.31	94.27	90.2(0 K), 92.2(298 K)[e]
$H_3CN(O)-O$	92.74	93.49	94.06	94.72	93.5(298 K)[b]
H_3CO-NO cis	38.87	40.08	42.91	44.12	41.8(298 K)[f]
H_3CO-NO trans	37.53	38.62	42.09	43.18	
ΔE(cis−trans)	1.35	1.54	0.82	1.01	0.62[g], 0.90[h], 0.75[i], 1.00[j]

[a] Temperature corrections in the present work are restricted to the rigid rotor harmonic oscillator model. [b] Kinetic measurement ref 49. [c] From the difference in heats of formation of CH_3NO_2 (−17.76 kcal/mol) and CH_3ONO (−15.85 kcal/mol), ref 50. [d] Reference 26. [e] From ΔH (kcal/mol) values for (0 K, 298 K): CH_3OH (−45.42, −48.04) from ref 51, CH_3O (5.9 ± 1.0, 4.0 ± 1.0) from ref 52, and CH_3 (35.6, 34.8 ± 0.3), OH (9.3, 9.39), H (51.63, 52.64), O (59.0, 60.04) from ref 53. [f] Reference 41. [g] Effusive beam ref 54. [h] Microwave ref 55. [i] Infrared spectrum ref 47. [j] Gas-phase NMR ref 56.

an alternative, more accurate bond energies can often be obtained with less computational expense computing the heat of reaction for an isodesmic reaction, since errors tend to cancel when the number of bonds is equal and the character of chemical bonding on the left- and right-hand side of the equation is close. This is what we have done for the example of cis CH_3O-NO. The isodesmic reaction to be considered is

$$HONO(cis) + CH_3O \rightarrow CH_3ONO(cis) + OH \qquad (1)$$

which probes internal consistency of bond energy data available for HO−NO compared with CH_3O-NO. The heats of reaction computed improving the single-particle basis set using the CCSD(T) approach are also summarized in Table 2. The method of convergence suggests that a value of 5.6 kcal/mol for this reaction is close to the basis set limit and gives our best estimate $D_e(CH_3O-NO,cis)$ of 46.2 kcal/mol. This value is only 1.3 kcal/mol smaller than the G2′(MP2) result obtained directly and 1.4 kcal/mol larger than the CCSD(T) + ΔMP2 result. Including the zero-point correction, we obtain 42.8 kcal/mol for $D°_{298}(CH_3O-NO,cis)$ and 41.8 kcal/mol for the trans conformer, in good agreement with kinetic measurements of 41.8 kcal/mol,[41] which must be interpreted at room temperature as a mixture of cis and trans.

Thus while for CH_3-O and CH_3O-NO the best theoretical values are between the CCSD(T) + ΔMP2 and the G2′(MP2)

TABLE 2: Summary of Calibration Calculations of Bond Energies D_e (kcal/mol) for CH_3-O and CH_3O-NO. Values for the Latter Obtained via Computing Heat of Isodesmic Reaction $\Delta_r H$, Eq 1, Are also Summarized

	D_e	
	CH_3-O	CH_3O-NO
B3LYP/6-31G*	95.10	43.51
CCSD(T)/6-311G**	82.95	39.82
CCSD(T)/6-311G**+ΔMP2	90.55	44.83
G2′(MP2)	93.26	47.54
CCSD(T)/cc-pVDZ	81.06	39.54
CCSD(T)/cc-pVTZ	87.77	43.81
CCSD(T)/cc-pVQZ	90.46	
CCSD(T)/cc-pV∞Z[a]	92.02	

	$D_e(CH_3O-NO)$[b]	
	ΔH	CH_3O-NO
CCSD(T)/6-311G**	5.84	45.89
CCSD(T)/6-311G**+ΔMP2	5.56	46.17
G2′(MP2)	5.56	46.17
CCSD(T)/cc-pVTZ	5.90	45.83

[a] Extrapolated value using the form A+B/(l+1/2)^4 as described in ref 40. [b] Using heat of reaction $\Delta_r H$: HONO + CH_3O → CH_3ONO + OH. For the best estimate of $D_e(CH_3O-NO)$ from the calculated heat of reaction, eq 1, we use D_e (HO−NO,cis) = 51.73 kcal/mol. (D_0(HO−NO,cis) = 47.61 kcal/mol from JANNAF tables.[53] ZPEs are obtained from ref 57 for OH, NO including anharmonic corrections and for cis HONO from refs 58, 59, who report fundamentals.

result, we find it reasonable to calibrate the B3LYP bond energies using the CCSD(T) level of theory with the MP2 basis set correction. If also the HLC to the G2′(MP2) approach is employed, the remaining sources of errors of 1−2 kcal/mol are not easy to interpret for these compounds.

Computed barriers for internal rotation about C−O and C−N bonds are summarized in Table 3. The experimental values[43−47,59−62] are also included. Thereby all coordinates are optimized at the B3LYP level. The saddle points were verified to carry one imaginary frequency. The B3LYP rotational barriers are in reasonable agreement with the CCSD(T) results. In particular nitromethane has a very weak potential barrier at all levels of theory and shows that internal rotation is nearly free, as has also been found in microwave studies.[42−45] At the CCSD(T) level the MP2 correction for one-particle basis set incompleteness is small, suggesting that the barrier height is not strongly affected by further improvements of the basis set for these compounds. However, this effect is largest for CH_3-OH with a ΔMP2 of 0.4 kcal/mol.

For cis CH_3ONO experimental work[46−48] suggests that the staggered rotational conformer is the ground state with a barrier for internal rotation of 2 kcal/mol, in good agreement with the CCSD(T) results. On the contrary, trans CH_3ONO has a much smaller barrier, less than 0.2 kcal/mol, which has made the determination of the equilibrium conformation and structural parameters from the microwave[46] and infrared measurements[47] difficult. The B3LYP structural data in comparison with experimental derived data[46,47] are summarized in Table 4 and show that there are significant changes of bond length and angles of both movements (1) when going from the cis to the trans conformer and (2) upon internal rotation from the staggered to eclipsed arrangement. The latter effect is important even for nearly free internal rotors such as trans CH_3ONO and CH_3NO_2 (Table 5). It is interesting to observe that for trans CH_3ONO our data yield the eclipsed structure as the ground state at all levels of theory. This can be interpreted to be stabilized due to the interaction of the lone pair of nitrogen with H−C (N−H

TABLE 3: Calibration Calculations for Rotational Barriers ΔE^{rot}. The B3LYP Values Are Computed with the 6-31G* Basis Set. In the CCSD(T) Calculations, the 6-311G and VTZ Sets Are Used. ΔMP2 Denotes the Basis Set Extension Contribution to the G2′(MP2) Approach. The Ground-State Rotational Conformer Staggered (s) or Eclipsed (e) Is Denoted in Parentheses**

	ΔE^{rot} (kcal/mol)				
structure	B3LYP	CCSD(T)/[a]6-311G**	CCSD(T)+ΔMP2	CCSD(T)/[a]VTZ	expt
CH_3-NO_2 (e)	0.003	−0.011	0.016		0.006[b]
CH_3-ONO cis (s)	1.42	2.16	2.03	1.99	2.26[c], 2.09[d], 1.91[e]
CH_3-ONO trans (e)	0.69	0.26	0.15		0.029[d], 0.061[d], 0.188[e]
CH_3-NO (e)	1.50	0.96	1.12	1.16	1.159[g], 1.4 ± 0.3[h]
CH_3-OH (s)	1.43	1.44	0.98	1.10	1.07[f]

[a] Computed at the B3LYP/6-31G* optimized geometry. Rotational transition states carry one imaginary frequency. [b] Refs 43, 44, 45. [c] Ref 47. [d] Ref 46. [e] Ref 60. [f] Ref 61. [g] Ref 62. [h] Ref 63.

TABLE 4: Summary of B3LYP Structural Data (Bond Lengths in Å, Angles in deg) for Conformers of Methyl Nitrite in Comparison with Measurements (Experimental Uncertainties in Parentheses)

	CH_3ONO				
	B3LYP		expt		
parameter	stag	ecl	A[a]	B[b]	C[b]
			cis CH_3-ONO		
$N-O_1$	1.191	1.186	1.182(5)	1.179(6)	1.181(5)
O_2-N	1.397	1.414	1.398(5)	1.420(8)	1.418(8)
$C-O_2$	1.439	1.438	1.437(5)	1.437(6)	1.436(6)
$C-H_1$	1.090	1.092	(1.09)[c]	1.090(3)	1.089
$C-H_{2,3}$	1.094	1.093	1.102(10)	1.090(3)	1.094
O_2NO	114.4	115.8	114.8(5)	114.5(6)	114.3(5)
CO_2N	115.5	118.1	114.7(5)	114.2(4)	114.5(4)
O_2CH_1	104.5	110.8	101.8(15)	102.4(4)	102.6(6)
$O_2CH_{2,3}$	110.8	107.6	109.9(5)	112.7(6)	110.4(3)
			trans CH_3-ONO		
$N-O_1$	1.182	1.179	1.164(5)	1.168(15)	1.170(15)
O_2-N	1.422	1.425	1.415(5)	1.452(8)	1.451(8)
$C-O_2$	1.435	1.432	1.436(5)	1.435[d]	1.435[d]
$C-H_1$	1.094	1.095	1.09[c]	1.092(19)	1.099(18)
$C-H_{2,3}$	1.094	1.094	1.09[c]	1.092(19)	1.099(18)
O_2NO	110.5	110.8	111.8(5)	110.3(13)	110.2(13)
CO_2N	109.7	110.3	109.9(5)	107.8(5)	107.8(5)
O_2CH_1	105.4	109.8	109.5[c]	101.3(22)	102.6(18)
$O_2CH_{2,3}$	111.0	108.7	109.5[c]	111.8(10)	111.0(10)

[a] Ref 46. [b] Ref 47. [c] Assumed. [d] Fixed.

TABLE 5: Geometry of Nitromethane in Comparison with Experiment (Bond Lengths in Å, Angles in deg)

	CH_3-NO_2		
	B3lYP		
parameter	stag	ecl	expt[a]
$C-N$	1.499	1.499	1.489
$N-O_1$	1.227	1.226	1.224
$N-O_2$	1.227	1.227	1.224
$C-H_1$	1.092	1.087	(1.089)
$C-H_{2,3}$	1.089	1.091	(1.089)
CNO_1	117.0	117.7	117.35
CNO_2	117.0	116.4	117.35
O_1NO_2	125.9	125.9	125.3
NCH_1	106.8	108.5	107.5
$NCH_{2,3}$	108.1	107.2	107.5
CO_1NO_2	177.9	180.0	

[a] Experimental data measured as an average over torsional angle of the methyl group from refs 43, 45.

distance 2.32 Å), which is impossible for the eclipsed structure of the cis conformer.

The B3LYP bond energies and stationary points of the potential hypersurfaces considered for CH_3 + O, OH, NO, and NO_2 are sufficiently accurate (a few kcal/mol for D_{298} and 1 kcal/mol for E^{rot}) and can be used to establish the trends for the larger cluster models for a diamond surface.

4.2. *tert*-Butyl and $C_{13}H_{21}$ + O, OH, NO, and NO_2. All structures have been fully optimized using B3LYP. Changes in geometry of the adsorbed species with the size of the cluster model are given in Table 6. $C_{13}H_{21}$ (Figure 1) is our best cluster model for a diamond (111) surface. C−C distances in $C_{13}H_{21}$ are in general longer than found for *tert*-butyl (larger distances from the central C atom to the $C_1C_2C_3$ plane) and show that *tert*-butyl structures are more planar without second-shell carbon atoms constraining the geometry. All angles C−X−Y for adsorbed molecules are larger in $C_{13}H_{21}$ than for *tert*-butyl by 1.2° (C−OH), 2.0° (C−NO), 3.9° (C−ONO,trans), 1.0° (C−NO_2), and 8.8° for C−ONO(cis). These changes indicate the importance of interactions between the surface atoms and adsorbed species, which is a limitation of the *tert*-butyl model but included in the $C_{13}H_{21}$ cluster model. As expected C−ONO-(cis) shows the largest effect. Both angles C−O−N and O−N−O increase; that is, the terminal O atom is pushed away from the surface.

Bond energy data are summarized in Table 7. Bond energies C−O and C−H for $C_{13}H_{21}$ and *tert*-butyl are similar, but neighboring C_mH_n bonds destabilize bonds of adsorbed molecules in the sequence C−OH (0.3 kcal/mol) < C−ONO,trans (4.6 kcal/mol), < C−NO (5.2 kcal/mol) < C−NO_2 (6.9 kcal/mol) < C−ONO,cis (9.4 kcal/mol). This is consistent with increasing repulsive interaction of the terminal atoms with second shell neighbors of the surface, hence depend mainly on sterical requirements. Thus in agreement with earlier theoretical work for C−H[48] and also C−F,[21] accurate parameters for molecular dynamics simulations such as geometrical, thermochemical data, and activation energies for abstraction of C atoms can advantagously be deduced using the *tert*-butyl model. On the other hand for an accurate description of the surface interaction of the molecules studied here, it is necessary to go beyond data derived from the *tert*-butyl-molecule potential hypersurface or from gas-phase experimental data.

Comparing the B3LYP value of 92.7 kcal/mol for the *tert*-butyl−H bond energy with the accurately known recommended value of 96.5 kcal/mol[27] indicates an error of 3.8 kcal/mol in absolute energies of *tert*-butyl−H (isobutane) relative to the *tert*-butyl radical. This slight error is expected to be also present for the results of the various directly calculated B3LYP bond energies *tert*-butyl−Y (Table 7), since it is clearly a defect of the relative description of the *tert*-butyl skeleton, irrelevant for C−Y bonds, and suggests the simple correction of adding 3.8 kcal/mol for *tert*-butyl−Y and similarly for $C_{13}H_{21}$−Y bond energies. In fact this shows that C−O and C−OH bond energies are significantly larger for *tert*-butyl (1.7, 3.2 kcal/mol) and $C_{13}H_{21}$ (3.7, 2.9 kcal/mol) than for CH_3, which indicates that the neighboring C_nH_m groups stabilize C−O and C−OH bonds more than the radical. Further, the bond energies C−NO, C−ONO, and C−NO_2 for *tert*-butyl are now closer to those for CH_3: about 1.2 kcal/mol lower for C−NO, 0.8 kcal/mol larger for C−ONO(trans), 2.7 kcal/mol lower for C−ONO(cis),

TABLE 6: Summary of B3LYP Structural Data for Adsorption of O, OH, NO, and NO_2 on Diamond, for the X = CH_3, *tert*-Butyl, and $C_{13}H_{21}$ Cluster Models (Bond Length in Å, Angles in deg). κ Denotes the Distance from the Central Carbon Atom C to the $C_1C_2C_3$ Plane (Figure 1)

compound	parameter	CH_3	$(CH_3)_3C$	$C_{13}H_{21}$
X	κ	0.158	0.231	
X−H	C−H	1.083	1.101	1.106
	κ		0.469	0.458
X−O	C−O	1.368	1.381	1.362
	κ		0.485	0.520
X−OH	C−O	1.419	1.439	1.443
stag	O−H	0.969	0.971	0.969
	C−O−H	107.6	107.3	108.1
	κ		0.474	0.494
X−OH	C−O	1.423	1.444	1.448
ecl[a]	O−H	0.966	0.968	0.967
	C−O−H	108.3	108.3	108.9
X−ONO	C−O	1.439	1.489	1.512
cis	O−N	1.397	1.385	1.383
stag	N═O	1.191	1.194	1.191
	O−N═O	114.4	116.4	118.1
	C−O−N	115.5	122.6	131.4
	κ		0.460	0.498
X−ONO	C−O	1.438	1.496	1.513
cis	O−N	1.414	1.394	1.387
ecl[a]	N═O	1.186	1.189	1.190
	O−N═O	115.8	117.8	118.6
	C−O−N	118.1	128.4	134.3
	κ		0.474	0.496
X−ONO	C−O	1.435	1.473	1.475
trans	O−N	1.422	1.408	1.411
stag[a]	N═O	1.182	1.187	1.186
	O−N═O	110.5	110.5	109.8
	C−O−N	109.7	112.3	118.1
	κ		0.454	0.492
X−ONO	C−O	1.432	1.471	1.477
trans	O−N	1.425	1.410	1.407
ecl	N═O	1.179	1.186	1.186
	O−N═O	110.8	110.3	109.9
	C−O−N	110.3	115.2	119.1
	κ		0.465	0.494
X−NO	C−N	1.487	1.520	1.507
ecl	N═O	1.211	1.210	1.213
	C−N═O	113.2	114.8	116.8
X−NO	C−N	1.503	1.538	1.520
stag[a]	N═O	1.210	1.210	1.214
	C−N═O	112.1	113.2	115.8
X−NO_2	C−N	1.499	1.550	1.553
stag	N−O	1.227	1.227	1.230
	O−N−O	125.9	124.7	122.7
	C−N−O	117.0	117.6	118.6
	κ		0.450	0.505
X−NO_2	C−N	1.499	1.550	1.555
ecl	N−O_1	1.226	1.226	1.229
	N−O_2	1.227	1.229	1.230
	O−N−O	125.9	124.7	122.6
	C−N−O_1	117.7	118.6	119.7
	C−N−O_2	116.4	116.7	117.7
	k		0.449	0.507

[a] Rotational transition state.

and 0.1 kcal/mol larger for C−NO_2. It is interesting to observe that for *tert*-butyl−ONO our theoretical result predicts the trans conformer to be about 2 kcal/mol lower in energy than cis *tert*-butyl−ONO, contrary to methylnitrite, where the cis conformer is the ground state.

Major computational effort is necessary for achieving more accurate bond energies beyond the B3LYP approach, employing higher levels of theory like the coupled-cluster method (CCSD(T) used in the calibration calculations for CH_3. However, as an alternative to direct calculation of bond energies, we always may compute the heat of an isodesmic reaction $\Delta_r H$, where the number and character of the bonds on the left- and right-hand side of the equation are close. This is what we do for the *tert*-butyl and $C_{13}H_{21}$ cluster models. For the example of the *tert*-butyl−Y bond energies the reaction we suggest is

$$CH_3{-}Y + t\text{-}C_4H_9{-}H \rightarrow CH_4 + t\text{-}C_4H_9{-}Y \qquad (2)$$

Our smallest cluster model CH_3 has common features in bonding with *tert*-butyl. The heats of (isodesmic) reaction computed for the various bond energies of *tert*-butyl and $C_{13}H_{21}$ are summarized in Table 8. The bond energies obtained using these values are the corrected ones, also summarized in Table 7. The most accurately known experimental datum for *tert*-butyl bond energies is the value of 39.8 ± 0.1 kcal/mol from predissociation dynamical studies for *tert*-butyl−NO,[64] in excellent agreement with the value 39.5± 1.5 kcal/mol from ref 26 and the value of 40.9 kcal/mol for the dissociation of *t*-C_4H_9O−NO from kinetic measurements[41,65] (assuming no activation barrier). For *tert*-butyl the corrected B3LYP bond energies are in good agreement with these values, which shows good internal consistency of the level of theory describing the bonds.

Our largest cluster model gives the best estimate for adsorption energies on diamond C(111). Bond energies decrease in

TABLE 7: Summary of B3LYP Bond Energies (kcal/mol). Corrected Values D_{298} (Corr) Are Obtained Using B3LYP Values for Isodesmic Reactions (Table 8)

	D_e	D_0	D_{298}	D_{298}(Corr)[a]	D_{298}(Expt)
H_3C−H	113.15	103.68	104.53		104.8[b]
$(H_3C)_3C$−H	100.53	91.29	92.72		96.5[b,c]
$C_{13}H_{21}$−H	101.82			97.79	
H_3C−NO_2	62.02	54.93	56.57		60.1[d]
$(H_3C)_3C$−NO_2	57.10	51.47	52.91	59.95	58.51[e]
$C_{13}H_{21}$−NO_2	50.17			53.02	
H_3C−NO	42.62	37.01	38.67		40.0 ± 0.8[e]
$(H_3C)_3C$−NO	36.61	32.42	33.74	38.58	39.8 ± 0.1[l], 39.51 ± 1.5[e]
$C_{13}H_{21}$−NO	31.38			33.35	
H_3C−O	95.10	90.82	91.92		90.8[f]
$(H_3C)_3C$−O	92.39	88.86	89.81	92.19	93.99[g]
$C_{13}H_{21}$−O	94.43			94.23	
H_3C−ONO trans	59.58	53.53	54.98		(57.2)[h]
$(H_3C)_3C$−ONO trans	55.08	50.84	51.99	57.72	
$C_{13}H_{21}$−ONO trans	50.51			53.15	
H_3C−ONO cis	61.16	54.89	56.53		58.2[h]
$(H_3C)_3C$−ONO cis	53.18	48.78	50.02	55.21	
$C_{13}H_{21}$−ONO cis	43.75			45.78	
H_3C−OH	95.80	87.59	89.55		92.2[i]
$(H_3C)_3C$−OH	93.61	87.02	88.91	95.07	96.35[j]
$C_{13}H_{21}$−OH	93.34			94.80	
$H_3CN(O)$-O	96.85	92.74	93.40		93.5[k]
$(H_3C)_3CN(O)$−O	97.94	93.87	94.67	94.77	
$C_{13}H_{21}N(O)$−O	96.24			93.07	
H_3CO−NO trans	41.94	37.53	38.55		(40.8)[h,k]
$(H_3C)_3CO$−NO trans	40.15	36.80	37.68	39.93	40.9 ± 0.8[k]
$C_{13}H_{21}O$−NO trans	33.55			33.03	
H_3CO−NO cis	43.51	38.87	40.08		41.8[k]
$(H_3C)_3CO$−NO cis	38.24	34.73	35.70	37.12	
$C_{13}H_{21}O$−NO cis	26.79			25.67	

[a] For obtaining the corrected values for the B3LYP *tert*-butyl bond energies using reactions 1−3 we take the recommended value for *t*-C_4H_9−H (refs 27, 28) and chose to take the experimental bond energy data for the CH_3 cluster model since this is close to the CCSD(T)+MP2 and G2′(MP2) results (Tables 1, 2). Our best estimate of $C_{13}H_{21}$ bond energies, eqs 4−6, use the corrected values for the *tert*-butyl cluster of this table. [b] Ref 28. [c] Ref 27. [d] Ref 49. [e] Ref 26. [f] From $\Delta_f H°_{298}$ for CH_3O (4.0 ± 1.0), ref 52, and CH_3 (34.8 ± 0.3), O (60.04). [g] From $\Delta_f H°_{298}$ (kcal/mol) for *t*-C_4H_9 (12.26), ref 27, and *t*-C_4H_9O (−21.70), ref 26. [h] From difference in $\Delta_f H°_{298}$ (kcal/mol) for CH_3NO_2 (−17.76), CH_3ONO (−15.85) from ref 50. (The cis isomer is more stable than trans by 0.7−1.0 kcal/mol, refs 54, 55, 47, 56.) [i] From $\Delta_f H°_{298}$ (kcal/mol) for CH_3OH (−48.04), OH (9.39), refs 51, 53. [j] From $\Delta_f H°_{298}$ (kcal/mol) for *t*-C_4H_9OH (−48.04), ref 66. [k] Refs 41, 65. [l] Ref 64.

TABLE 8: Summary of B3LYP Computed Heats of Reaction $\Delta_r H$ (kcal/mol) for the Calculation of Bond Energies X−Y, XN(O)−O, and XO−NO (X = *t*-C_4H_9, $C_{13}H_{21}$ and Y = NO_2, NO, O, ONO, OH). The Values Refer to 298 K[a]

(1)	$CH_3-Y + t\text{-}C_4H_9-H \rightarrow CH_4 + t\text{-}C_4H_9-Y$
(2)	$CH_3N(O)-O + t\text{-}C_4H_9NO \rightarrow CH_3NO + t\text{-}C_4H_9N(O)-O$
(3)	$CH_3O-NO + t\text{-}C_4H_9O \rightarrow CH_3O + t\text{-}C_4H_9O-NO$
(4)	$t\text{-}C_4H_9-Y + t\text{-}C_{13}H_{21} \rightarrow t\text{-}C_4H_9 + t\text{-}C_{13}H_{21}-Y$
(5)	$t\text{-}C_4H_9N(O)-O + t\text{-}C_{13}H_{21} \rightarrow t\text{-}C_4H_9NO + t\text{-}C_{13}H_{21}N(O)-O$
(6)	$t\text{-}C_4H_9O-NO + t\text{-}C_{13}H_{21} \rightarrow t\text{-}C_4H_9O + t\text{-}C_{13}H_{21}O-NO$

	X = *t*-C_4H_9			X = *t*-$C_{13}H_{21}$	
no.	bond	$\Delta_r H$	no.	bond	$\Delta_r H$
(1)	X−NO_2	−8.15	(4)	X−NO_2	6.93
(1)	X−NO	−6.88	(4)	X−NO	5.23
(1)	X−O	−9.69	(4)	X−O	−2.04
(1)	X−ONO trans	−8.82	(4)	X−ONO trans	4.57
(1)	X−ONO cis	−5.31	(4)	X−ONO cis	9.43
(1)	X−OH	−11.17	(4)	X−OH	0.27
(2)	XN(O)−O	−1.26	(5)	XN(O)−O	1.70
(3)	XO−NO trans	0.87	(6)	XO−NO trans	6.60
(3)	XO−NO cis	4.38	(6)	XO−NO cis	11.45

[a] For reactions 4−6 we neglect the change in zero-point corrections for bond energies when increasing the size of the cluster model from *t*-C_4H_9 to $C_{13}H_{21}$. We estimate this error as less than 1 kcal/mol.

TABLE 9: Summary of B3LYP Calculations for Rotational Barriers ΔE^{rot}. The Ground-State Rotational Conformer Staggered (s) or Eclipsed (e) Is Denoted in Parentheses

	ΔE^{rot} (kcal/mol)		
structure	X = CH_3	*t*-C_4H_9	*t*-$C_{13}H_{21}$
X−NO_2	0.00(e)	0.26(e)	0.26(s)
X−ONO cis	1.42(s)	4.97(s)	0.60(s)
X−ONO trans	0.69(e)	1.40(s)	0.77(s)
X−NO	1.50(e)	1.36(e)	0.57(e)
X-OH	1.43(s)	1.58(s)	0.97(s)

the sequence C−H (98 kcal/mol) > C−OH (95 kcal/mol) > C−O (94 kcal/mol) > C−ONO,trans (53 kcal/mol) > NO_2 (53 kcal/mol) > C−ONO,cis (45 kcal/mol) > C−NO (30 kcal/mol). The energy of dissociation

$$C_{13}H_{21}ONO \rightarrow C_{13}H_{21}O + NO(X\,^2\Pi) \qquad (3)$$

is 33.0 kcal/mol for the trans and 25.7 kcal/mol for the cis conformer, i.e., much smaller than for *tert*-butyl or CH_3.

Barriers for internal rotations arround the C−N and C−O bonds are summarized in Table 9. The values for $C_{13}H_{21}$ are smaller than for *tert*-butyl. This is consistent with the trend that the C−NO_2, C−ONO, C−NO, and C−OH bond energies are smaller. In fact all the computed barrier heights for $C_{13}H_{21}$ are less than 1 kcal/mol and only about 0.3 kcal/mol for C−NO_2. This means that internal rotation is almost free. For C−NO all 3-fold rotors CX_3−NO studied so far have eclipsed ground-state geometries, which is also the case for $C_{13}H_{21}$−NO. In good agreement with experimental work,[64] the rotational B3LYP barriers for CH_3−NO and *tert*-butyl−NO are very close. It is interesting to observe that our data suggest a large barrier of 5.0 kcal/mol for cis *tert*-butyl−ONO. For all clusters employed for C−ONO(cis) we found the staggered rotational conformer as the ground state. For *tert*-butyl the distance of the terminal O atom with the two closest symmetrical identical H atoms is 2.42 and 2.52 Å for CH_3. This may indicate that the interaction of terminal O with H−C stabilizes the staggered compound relatively more for *tert*-butyl but primarily depends on sterical requirements, largest for eclipsed *tert*-butyl−ONO(cis), which has O−N−O and C−O−N angles 2° and 10° larger than for CH_3ONO(cis,eclipsed) and 1° and 4° larger than for staggered *tert*-butyl−ONO(cis) (Table 6).

5. Summary and Conclusion

It is anticipated that these data for hydrocarbons Y−CH_3, Y−$C(CH_3)_3$, and Y−C_{13} H_{21} will be used to calibrate the parameters of the potential energy functions of σ bonds C−Y required to model the interaction of the oxygen-containing species Y with a diamond surface for simulation of plasma−surface interaction and etching.

The calibration studies show that bond dissociation energies for C−O, C−OH, C−NO_2, C−ONO, C−NO, CO−NO, and CN(O)-O and rotational barriers can accurately be derived using the B3LYP approach. For Y−$C_{13}H_{21}$ these have been determined at the B3LYP level to model the surface bonding of small oxygen-containing radicals on an active site of a hydrogenated diamond C(111) surface. The C−O bond energy for $C_{13}H_{21}$ is 2 kcal/mol larger than for *tert*-butyl. On the contrary, the values for C−NO_2, C−ONO, C−NO, and CO−NO are lower by about 6−10 kcal/mol compared with *tert*-butyl. This shows that the effect of the second nearest neighbor is large in these cases and the significance of steric effects between the surface and Y. For an accurate description of the interaction of molecules with the diamond surface it is necessary to go beyond small hydrocarbon models. Rotational barriers for chemisorbed OH, NO_2, ONO, and NO are computed to be less than about 1 kcal/mol and show that rotation is essentially free. Combining the trends observed for the small cluster models yields our best absolute values for adsorption energies on a radical site of hydrogen-terminated diamond (111): Bond energies decrease in the sequence C−H (98 kcal/mol) > C−OH (95 kcal/mol) > C−O (94 kcal/mol) > C−ONO,trans (53 kcal/mol) > C−NO_2 (53 kcal/mol) > C−ONO,cis (45 kcal/mol) > C−NO (30 kcal/mol). Dissociation energies of cis CO−NO and trans CO−NO are small (26 kcal/mol, 33 kcal/mol). The value for CN(O)−O is 93 kcal/mol, hence 20 kcal/mol larger than for N(O)−O.

Acknowledgment. The author would like to acknowledge helpful discussions with C. W. Bauschlicher.

References and Notes

(1) Himpsel, F. J.; Knapp, J. A.; van Vecten, J. A.; Eastman, D. E. *Phys. Rev. B* **1979**, *20*, 624.

(2) Geis, M. W.; Gregory, J. A. Pate, B. B. IEEE Trans. Electron. Dev. **1991**, *38*, 3.619.

(3) Gilmour, A. S. *Principles of Traveling Wave Tubes*; Artech House: Norwood, MA, 1994; Chapter 18.

(4) Chu, X.; et al., *Ind. Eng. Chem. Res.* **1993**, *32* (7), 1359.

(5) Harada, K. *J. Appl. Polym. Sci.* **1981**, *26*, 1961.

(6) Geis, M. W.; Angus, J. C. *Sci. Am.* **1992**, *10*, 84.

(7) Tanaguchi, J.; Miyamoto, I. Beam-Solid Interactions for Material Synthesis and Characterization, Symp., Boston, MA, *Proc. Mater. Res. Soc.* **1995**, *354*, 711.

(8) Rawles, R. E.; Evelyn, M. P. D. In Diamond, SiC and Nitride Wide Bandgap Semiconductor Symp., Pittsburgh, *Mater. Res. Soc.* **1994**, 279.

(9) Oshashi, H.; Ishiguro, E.; Susano, T.; Shobatake, K. *Appl. Phys. Lett.* **1996**, *68*, 3713.

(10) Chu, C. J.; Pang, C.; Margrave, J. L.; Hange, R. H.; *Diamond Relat. Mater.* **1995**, *4*, 1317.

(11) Kiyohara, S.; Miyamoto, I. *J. Jpn. Soc. Precise Eng.* **1996**, *62*, 1459.

(12) Yourbrough, W. A.; Messier, R. *Science* **1990**, *24*, 688.

(13) Tolt, Z. L. Heatarly, L.; Clausing, R. E.; Feigerle, C. S. *J. Appl. Phys.* **1997**, *81*, 1536.

(14) Ikeda, M.; Mizuno, E.; Hori, M.; Goto, T.; Yamada, K. *Jpn. J. Appl. Phys. Part 1*, **1996**, *35* (9A) 4826.

(15) Geis, M. W.; Pang, S. W.; Efremow, N. E.; Lincoln, G. A.; Johnson, G. D.; Goodhue, W. D. In *Handbook of Ion Beam Processing Technology*;

Cuomo, J. J., Rossnagel, S. M., Kaufmann, H. R., Eds.; Noyes Publications: Park Ridge, NJ, 1989.

(16) Winters, H. F.; Coburn, J. W.; Chuang, T. J. *J. Vac. Sci. Technol. B 1983, 1,* 469.

(17) Winters, H. F.; Coburn, J. W. In *Plasma Synthesis and Etching of Electronic Materials*; (Chang, R. P. H.; Abeles, B.) Eds.; *Mater. Res. Soc. Symp. Proc*. Vol 38; Material Research Society: Pittsburgh, 1985.

(18) Mamin, H. J.; Terris, B. D.; Fan, L. S.; Hoen, S.; Barrett, R. C.; Rugar, D. *IBM J. Res. Dev.* **1995**, *39*, 681.

(19) Bauschlicher, C. W.; Ricca, A.; Merkle, R. *Nanotechnology* **1997**, *8*, 1.

(20) Avouris, Ph.; Walkup, R. W.; Rossi, A. R.; Akpati, H. C.; Nordlander, P.; Shen, T.-C.; Lyding, J. W.; Abeln, G. C. *Surf. Sci*. **1996**, *363*, 368.

(21) Thümmel, H. T.; Bauschlicher, C. W. *J. Phys. Chem*. **1997**, *101*, 1188.

(22) Thümmel, H. T.; Bauschlicher, C. W. To be published.

(23) De Vita, A.; Galli, G.; Canning, A.; Car, R. *Nature* **1996**, *379*, 523.

(24) Pate, B. B.; *Surf. Sci.* **1986**, *165*, 83.

(25) Hamza, A. V.; Kubiak, G. D.; Stulen, R. H. *Surf. Sci*. **1988**, *206*, L833.

(26) McMillen, D. F.; Golden, D. M.; *Annu. Rev. Phys. Chem*. **1982**, *33*, 493.

(27) Seakins, P. W.; Pilling, M. J.; Niiranen, J. T.; Gutman, D.; Krasnoperov, L. N. *J. Phys. Chem.* **1992**, *96*, 9847.

(28) Berkowitz, J.; Ellison, G. B.; Gutmann, D. *J. Phys. Chem.* **1994**, *98*, 2744.

(29) Stevens, P. J.; Devlin, F. J.; Chablowski, C. F.; Frisch, M. J. *J. Phys. Chem*. **1994**, *98*, 11623.

(30) Bartlett, R. J. *Annu. Rev. Phys. Chem*. **1981**, *32*, 359.

(31) Raghavachari, K.; Trucks, G. W.; Pople, J. A.; Head-Gordon, M. *Chem. Phys. Lett*. **1989**, *157*, 479.

(32) Frisch, M. J.; Pople, J. A.; Binkley, J. S. *J. Chem. Phys.* **1984**, *80*, 3265 and references therein.

(33) Dunning, T. H., Jr., *J. Chem. Phys.* **1989**, *90*, 1007.

(34) Curtiss, L. A.; Raghavachari, K.; Trucks, G. W.; Pople, J. A. *J. Chem. Phys.* **1991**, *94*, 17221.

(35) Bauschlicher, C. W.; Partridge, H. *J. Chem. Phys*. **1995**, *103*, 1788.

(36) Frisch, M. J.; Trucks, G. W.; Schlegel, H. B.; Gill, P. M. W.; Johnson, B. G.; Robb, M. A.; Cheeseman, J. R.; Keith, T.; Petersson, G. A.; Montgomery, J. A.; Raghavachari, K.; Al-Laham, M. A.; Zakrzewski, V. G.; Ortiz, J. V.; Foresman, J. B.; Cioslowski, J.; Stefanov, B. B.; Nanayakkara, A.; Challacombe, M.; Peng, C. Y.; Ayala, P. Y.; Chen, W.; Wong, M. W.; Andres, J. L.; Replogle, E. S.; Gomperts, R.; Martin, R. L.; Fox, D. J.; Binkley, J. S.; Defrees, D. J.; Baker, J.; Stewart, J. P.; Head-Gordon, M.; Gonzalez, C.; Pople, J. A. *Gaussian 94*, Revision D.1; Gaussian, Inc.: Pittsburgh, PA, 1995.

(37) MOLPRO 96 is an ab initio quantum chemistry package by Werner, H. J.; Knowles, P. J. with contributions from Almlöf, J.; Amos, R. D.; Deegan, M. J. O.; Elbert, S. T.; Hampel, C.; Meyer, W.; Peterson, K. A.; Pitzer, R. M.; Stone, A. J.; Taylor, P. R.; Lindh, R.

(38) Hampel, C.; Peterson, K. A.; Werner, H. J. *Chem. Phys. Lett*. **1992**, *190*, 1.

(39) Bauschlicher, C. W. Ricca, A.; Partridge, H.; Langhoff, S. T. Chemistry by density functional theory. Partridge, H.; Langhoff, S. R. In *Recent Advances in Density Functional Methods, Part II;* Chong, D. P., Ed.; World Scientific Publishing Co.: Singapore, 1997.

(40) Martin, J. M. L. *Chem. Phys. Lett*. **1996**, *259*, 669.

(41) Batt, L.; Christie, K.; Milne, R. T.; Summers, A. *J. Int. J. Chem. Kinet*. **1974**, *6*, 877.

(42) Cavagnat, D.; Lespade, L.; Lapouge, C. *J. Chem. Phys.* **1995**, *103*, 10502.

(43) Cox, A. P.; Waring, S. *J. Chem. Soc., Faraday Trans.* **1972**, *2*, 1060.

(44) Cox, A. P. *J. Mol. Struct.* **1983**, *97*, 61.

(45) Sorensen, G. O.; Pedersen, T.; Dreizler, H.; Guarnieri, A.; Cox, A. P. *J. Mol. Struct*. 97 1983 61.

(46) Turner, P. H.; Corkhill, M. J.; Cox, A. P. *J. Phys. Chem.* **1979**, *83*, 1473.

(47) Van der Veken, B. J.; Maas, R.; Guirgis, G. A.; Stidham, H. D.; Sheehan, T. G.; Durig, J. R. **1990**, *94*, 4029.

(48) Page, M.; Brenner, D. W. *J. Chem. Soc.* **1991**, *113*, 3270.

(49) Butler, L. J.; Krajnovich, Q.; Lee, Y. T.; Ondrey, G.; R. Berson *J. Chem. Phys*. **1983**, *79*, 1708.

(50) Pedley, J. B.; Naylor, R. D.; Kirby, S. P. *Thermochemical Data of Organic Compounds*; Chapman and Hall: London, 1986.

(51) Wagman, D. D. Evans, W. H.; Parker, V. B.; Schumm, S. H.; Halow, I.; Bailey, S. M.; Churney, K. L.; Nutall, R. J. *J. Phys. Chem. Ref Data* **1982**, *11*, Suppl. 1.

(52) Ruscic, B.; Berkowitz, J. *J. Chem. Phys*. **1991**, *95*, 4033.

(53) Chase, M. W.; Davies, C. A.; Downey, J. R.; Frurip, D. J.; McDonald, R. A.; Syverud, A. N. *J. Phys. Chem. Ref. Data* **1985**, *14*, Suppl. 1.

(54) Felder, P.; Ha, T.-K.; Dwivedi, A. M.; Günthard, Hs H. *Spectrochim. Acta* **1981**, *37A*, 337.

(55) Ghosh, P. N.; Bauder, A.; Günthard, Hs. H. *Chem. Phys. Lett.* **1980**, *53*, 39.

(56) Chauvel, J. P.; True, N. S. *J. Phys. Chem.* **1983**, *87*, 1622.

(57) Huber, K. P.; Herzberg, G. *Constants of Diatomic Molecules*; Van Nostrand: New York, 1979.

(58) Deeley, C. M.; Mills, I. M. *Mol. Phys*. **1985**, *54*, 23.

(59) Murto, J.; Rasanen, M.; Spiala, A. A.; Lotta, T. *J. Mol. Struct*. **1985**, *122*, 213.

(60) Gwinn, W. D.; Anderson, R. J.; Stelman, D. *Bull. Am. Phys. Soc*. **1968**, *13*, 831.

(61) Ivash, E. V.; Dennison, D. M. *J. Chem. Phys*. **1953**, *21*, 1804.

(62) van Eijck, B. P. *J. Mol. Spectrosc.* **1982**, *91*, 348.

(63) Ernsting, N. P.; Pfab, J.; Römelt, J. *J. Chem. Soc., Faraday Trans.* **1978**, *2*, 2286.

(64) Noble, M.; Quian, C. X. W.; Reisler, H.; Wittig, C. *J. Chem. Phys*. **1986**, *85*, 5763.

(65) Batt, L.; Milne, R. T. *Int. J. Chem. Kinet*. **1976**, *8*, 59.

(66) Lias, S. G.; Bartmess, J. E.; Liebman, J. F.; Holmes, J. L.; Levin, R. D.; Mallard, W. G. *J. Phys. Chem. Ref. Data*, **1988**, *17*, Suppl. 1.